Competitive Absorption and Inefficient Exciton Harvesting: Lessons Learned from Bulk Heterojunction Organic Photovoltaics Utilizing the Polymer Acceptor P(NDI2OD-T2)

*Zhi Li, Jason D. A. Lin, Hung Phan, Alexander Sharenko, Christopher M. Proctor, Peter Zalar, Zhihua Chen, Antonio Facchetti, and Thuc-Quyen Nguyen**

Organic solar cells utilizing the small molecule donor 7,7′-(4,4-bis(2-ethylhexyl)-4H-silolo[3,2-b:4,5-b′]dithiophene-2,6-diyl)bis(6-fluoro-4-(5′-hexyl-[2,2′-bithiophen]-5-yl)benzo[c][1,2,5] thiadiazole) (*p*-DTS(FBTTh$_2$)$_2$ and the polymer acceptor poly{[N,N′-bis(2-octyldodecyl)-1,4,5,8-naphthalenedicarboximide-2,6-diyl]-alt-5,5′-(2,2′-bithiophene)}(P(NDI2OD-T2)) are investigated and a power conversion efficiency of 2.1% is achieved. By systematic study of bulk heterojunction (BHJ) organic photovoltaic (OPV) quantum efficiency, film morphology, charge transport and extraction and exciton diffusion, the loss processes in this blend is revealed compared to the blend of [6,6]-phenyl-C71-butyric acid methyl ester (PC$_{71}$BM) and the same donor. An exciton diffusion study using Förster resonant energy transfer (FRET) shows the upper limit of the P(NDI2OD-T2) exciton diffusion length to be only 1.1 nm. The extremely low exciton diffusion length of P(NDI2OD-T2), in combination with the overlap in donor and acceptor absorption, is then found to significantly limit device performance. These results suggest that BHJ OPV devices utilizing P(NDI2OD-T2) as an acceptor material will likely be limited by its low exciton diffusion length compared to devices utilizing functionalized fullerene acceptors, especially when P(NDI2OD-T2) significantly competes with the donor molecule for photon absorption.

1. Introduction

In the past few years, solution-processed small molecule donor bulk heterojunction (BHJ) solar cells have made remarkable progress with power conversion efficiencies (PCEs) up to 8%.[1–13] These impressive PCEs have all been achieved using a fullerene derivative as the electron acceptor. Although fullerene acceptors have significant advantages with respect to efficient charge separation and generation of free carriers, large-scale use of fullerene derivatives may be hindered by the difficulty associated with their purification.[14,15] Purifying fullerenes and fullerene derivatives normally requires specialized equipment such as high-performance liquid chromatography which limits their scalability and raises their cost.[16,17] Moreover, although C_{70} derivatives (PC$_{71}$BM) show enhanced absorption in the blue region compared to C_{60} derivatives (PC$_{61}$BM),[18] it is still difficult to extend the absorption of fullerene derivatives into the red and near-infrared regions of the solar spectrum that could potentially contribute to photocurrent. For these reasons, a number of non-fullerene acceptor materials have been synthesized with the hope of replacing PCBM in BHJ solar cells.[19–30]

One alternative electron acceptor is poly{[N,N′-bis(2-octyldodecyl)-1,4,5,8-naphthalenedicarboximide-2,6-diyl]-alt-5,5′-(2,2′-bithiophene)} (P(NDI2OD-T2)),[31] a naphthalenediimide based high mobility n-type semiconducting polymer. As an acceptor material, it has several favorable properties: 1) high field-effect electron mobility

Z. Li, J. D. A. Lin, H. Phan, Dr. P. Zalar, Prof. T.-Q. Nguyen
Center for Polymer and Organic Solids
Department of Chemistry and Biochemistry
University of California Santa Barbara
Santa Barbara, CA 93106, USA
E-mail: quyen@chem.ucsb.edu
Dr. A. Sharenko, C. M. Proctor
Materials Department
University of California Santa Barbara
Santa Barbara, CA 93106, USA
Dr. Z. Chen, Dr. A. Facchetti
Polyera Corporation
8045 Lamon Avenue
Skokie, IL 60077, USA
Dr. A. Facchetti
Department of Chemistry
Northwestern University
Evanston, IL 60208–3113, USA
Prof. T.-Q. Nguyen
Department of Chemistry
Faculty of Science
King Abdulaziz University
Jeddah, Saudi Arabia

DOI: 10.1002/adfm.201401367

up to 0.85 $cm^2\ V^{-1}\ s^{-1}$[32] and diode electron mobility of $5 \times 10^{-4}\ cm^2\ V^{-1}\ s^{-1}$ with trap-free transport behavior;[33] 2) a reduced optical band gap (1.45 eV) compared to fullerene derivatives (≈2 eV);[34,35] and 3) a lowest unoccupied molecular orbital (LUMO) energy of 4.0 eV which is lower than the LUMO of some donor polymers and small molecules to ensure efficient photoinduced charge separation at donor/acceptor interfaces. Nevertheless, to date, polymer BHJ solar cells using P(NDI2OD-T2) as an electron acceptor have not performed as well as those with PCBM acceptors, mainly due to low short-circuit current densities (J_{sc}).[36–38] The poor performance may be the result of large scale phase separation.[35] Previous reports suggest preaggregation of P(NDI2OD-T2) in solution and relatively low charge mobilities as contributing factors to poor device performance.[39,40] On the other hand, physical mixtures of small-molecules and P(NDI2OD-T2) have been studied by Wunsch et al. showing that the morphology can be controlled by blend composition. This finding suggested that small molecules may be used with P(NDI2OD-T2) to fine tune film morphology and thereby optimize solar cell performance.[41]

Here, we investigate BHJ solar cell performance using P(NDI2OD-T2) as an electron acceptor with a small molecule donor material: 7,7′-(4,4-bis(2-ethylhexyl)-4H-silolo[3,2-b:4,5-b′]dithiophene-2,6-diyl)bis(6-fluoro-4-(5′-hexyl-[2,2′-bithiophen]-5-yl)benzo[c][1,2,5] thiadiazole), *p*-DTS(FBTTh$_2$)$_2$. The chemical structures and energy levels of the two compounds are shown in **Figure 1**. We hypothesize that the use of a small molecule donor material may mitigate some of the large-scale phase separation observed in polymer:P(NDI2OD-T2) blends.[36] We selected *p*-DTS(FBTTh$_2$)$_2$ as the donor material because of its excellent performance in solar cells using $PC_{71}BM$ as an electron acceptor, achieving PCEs of up to 8%.[2,21,42–46] The quantum efficiency, film morphology, charge transport and extraction and exciton diffusion are systematically studied in order to understand what factors limit the final performance of *p*-DTS(FBTTh$_2$)$_2$:P(NDI2OD-T2) BHJ OPV devices.

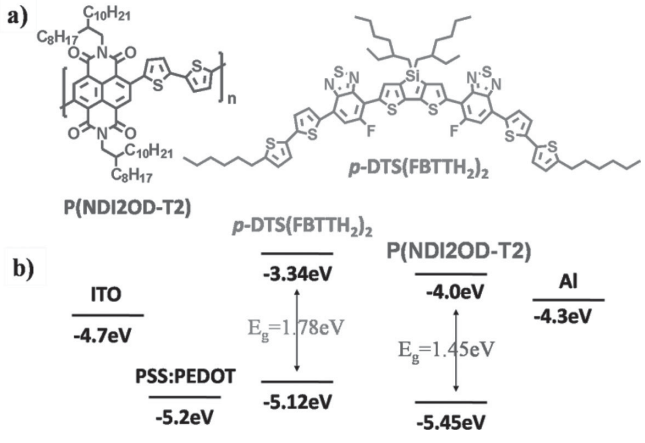

Figure 1. a) Chemical structures of donor *p*-DTS(FBTTh$_2$)$_2$ and acceptor P(NDI2OD-T2). b) The energy levels of the different BHJ components.

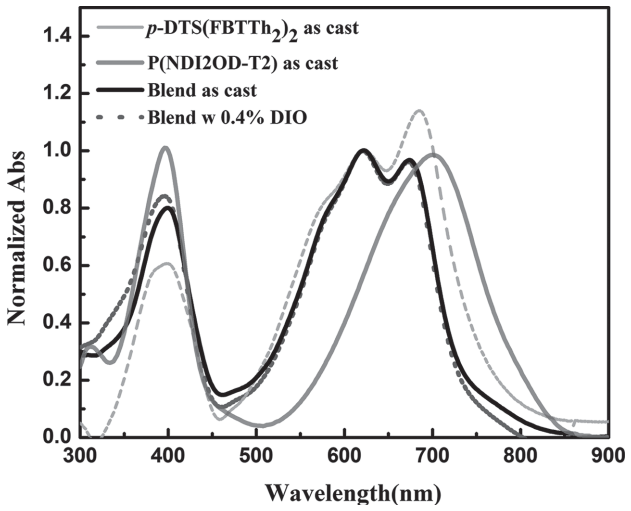

Figure 2. Film absorption spectra of pristine *p*-DTS(FBTTh$_2$)$_2$ and P(NDI2OD-T2), blend of *p*-DTS(FBTTh$_2$)$_2$:P(NDI2OD-T2) with and without 0.4% DIO.

2. Results and Discussion

The chemical structures and energy levels of *p*-DTS(FBTTh$_2$)$_2$ and P(NDI2OD-T2) as measured by cyclic voltammetry are shown in Figure 1. P(NDI2OD-T2)'s LUMO energy level is at 4.0 eV which provides a ≈0.64 eV offset from the LUMO of *p*-DTS(FBTTh$_2$)$_2$ for electron transfer from donor to acceptor.[2,31] In addition, hole transfer from P(NDI2OD-T2) to *p*-DTS(FBTTh$_2$)$_2$ is likely favorable, based on the 0.32 eV offset between the HOMO of *p*-DTS(FBTTh$_2$)$_2$ and P(NDI2OD-T2). P(NDI2OD-T2) has a band gap of 1.45 eV, slightly less than that of *p*-DTS(FBTTh$_2$)$_2$ (1.67 eV). In **Figure 2**, the thin-film absorption spectra are shown for *p*-DTS(FBTTh$_2$)$_2$, P(NDI2OD-T2) and the 3:2 donor:acceptor blend with and without 0.4% v/v 1,8-diiodooctane (DIO). The absorption spectra of pristine *p*-DTS(FBTTh$_2$)$_2$ and P(NDI2OD-T2) have typical absorption characteristics for donor–acceptor type conjugated polymers, with π–π^* transitions and the intramolecular charge transfer (ICT) transition in the ranges of 300–450 and 450–800 nm, respectively. The film absorption coefficients are comparable for pristine P(NDI2OD-T2) and *p*-DTS(FBTTh$_2$)$_2$, $5.3 \times 10^3\ cm^{-1}$ and $8.7 \times 10^3\ cm^{-1}$. Specifically, *p*-DTS(FBTTh$_2$)$_2$ has a strong π–π stacking absorption peak at 675 nm. Previous studies have shown that *p*-DTS(FBTTh$_2$)$_2$'s ICT and π–π^* bands can be red-shifted by the addition of DIO, indicating increased solid state order in the film.[2,43] In this work, when *p*-DTS(FBTTh$_2$)$_2$ is blended with P(NDI2OD-T2), the vibronic peak of *p*-DTS(FBTTh$_2$)$_2$ is weakened compared to pristine *p*-DTS(FBTTh$_2$)$_2$ suggesting reduced solid state order of *p*-DTS(FBTTh$_2$)$_2$ in the blend. It is difficult to infer structural information about *p*-DTS(FBTTh$_2$)$_2$ or P(NDI2OD-T2) from the blend absorption spectra because of the significant overlap between the absorption spectra of pristine donor and acceptor. Furthermore, the addition of a small amount DIO has no significant effect on the blend film absorption profile. The absorption spectra of pristine P(NDI2OD-T2) and P(NDI2OD-T2) with DIO are shown in Figure S1 of the Supporting Information.

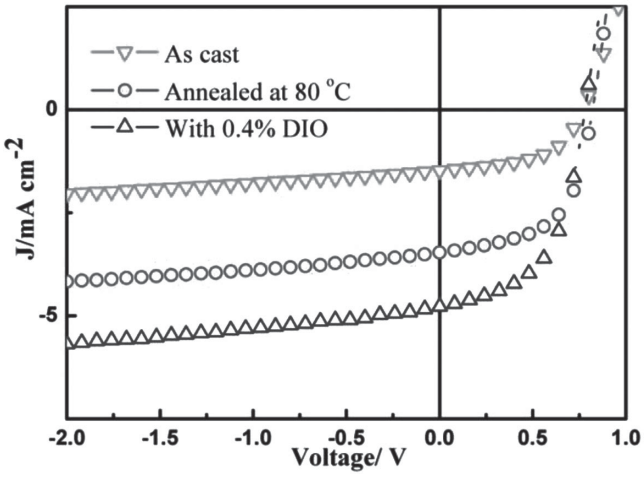

Figure 3. *J–V* characteristics of *p*-DTS(FBTTh$_2$)$_2$:P(NDI2OD-T2) solar cell devices prepared with different processing conditions: as cast, annealed and with 0.4% v/v DIO. Devices were tested with 100 mW cm^{-2} light intensity.

DIO does not have much effect on the absorption of pristine P(NDI2OD-T2).

Solar cell devices were fabricated and investigated with different donor:acceptor ratios, annealing temperatures, DIO content and cathodes (see Figures S2-S6 of the SI). As shown in **Figure 3**, the best performance is achieved using the architecture of ITO/PEDOT:PSS/3:2 w:w *p*-DTS(FBTTh$_2$)$_2$:P(NDI2OD-T2)/Al. The active layer was spun-coat from an 80 °C chlorobenzene solution. As shown in Figure 3 and **Table 1**, as cast BHJ blends exhibit an open-circuit voltage (V_{oc}) of 0.77 V which is comparable to that of *p*-DTS(FBTTh$_2$)$_2$:PC$_{71}$BM system, but the J_{sc} is very low, 1.48 mA cm^{-2}. After thermal annealing at 80 °C, the J_{sc} increases to 3.46 mA cm^{-2}. By processing with 0.4% v/v DIO, the J_{sc} increases further to 5.06 mA cm^{-2}. The V_{oc} and the fill factor (*FF*) remain relatively constant for all three device processing conditions (Table 1). Thus, improvement in device performance is mainly due to changes in the J_{sc} with PCEs of 0.61%, 1.64% and 2.11% for the as cast, annealed and additive processed devices, respectively. Although P(NDI2OD-T2)

Table 1. Device parameters of *p*-DTS(FBTTh$_2$)$_2$:P(NDI2OD-T2) solar cells.

	V_{oc} [V]	J_{sc} [mA cm^{-2}]	*FF*	PCE [%]
As cast	0.77	1.48	0.54	0.61
Annealed	0.82	3.46	0.57	1.64
With 0.4% DIO	0.79	5.06	0.53	2.11

has stronger absorption than PCBM, which should potentially allow for an increased J_{sc} compared to *p*-DTS(FBTTh$_2$)$_2$:PC$_{71}$BM devices, the J_{sc} of *p*-DTS(FBTTh$_2$)$_2$:P(NDI2OD-T2) is less than half of the J_{sc} of the *p*-DTS(FBTTh$_2$)$_2$:PC$_{71}$BM devices.[2,42] Generally, the PCE of an organic BHJ solar cell depends on several processes: photon absorption, exciton diffusion, charge generation, charge transport, and charge extraction. In order to understand the origin of the relatively low J_{sc}, we first focus our attention on the internal quantum efficiency (IQE) of the optimized *p*-DTS(FBTTh$_2$)$_2$:P(NDI2OD-T2) solar cells.

2.1. Internal Quantum Efficiency of *p*-DTS(FBTTh$_2$)$_2$:P(NDI2OD-T2)

The external quantum efficiency (EQE) of an optimized *p*-DTS(FBTTh$_2$)$_2$:P(NDI2OD-T2) device is shown in **Figure 4**a. Notably, the EQE of *p*-DTS(FBTTh$_2$)$_2$:P(NDI2OD-T2) only reaches a maximum value of 23%. To resolve how much of this can be attributed to losses not related to absorption, the IQE was determined. The IQE of a solar cell is defined as the percentage of absorbed photons that are successfully converted to current. We followed the procedure of Burkhart et al. to determine the number of photons absorbed in the active layer.[47] In this technique, the total device absorption is measured and the parasitic absorption from the contacts (glass, ITO, PEDOT:PSS, and Al) is calculated using a transfer matrix model. The active layer absorption is then taken to be the total absorption minus the parasitic absorption. As expected, the active layer absorption matches very well with the wavelength-dependent EQE (Figure 4a) leading to a relatively wavelength-independent IQE

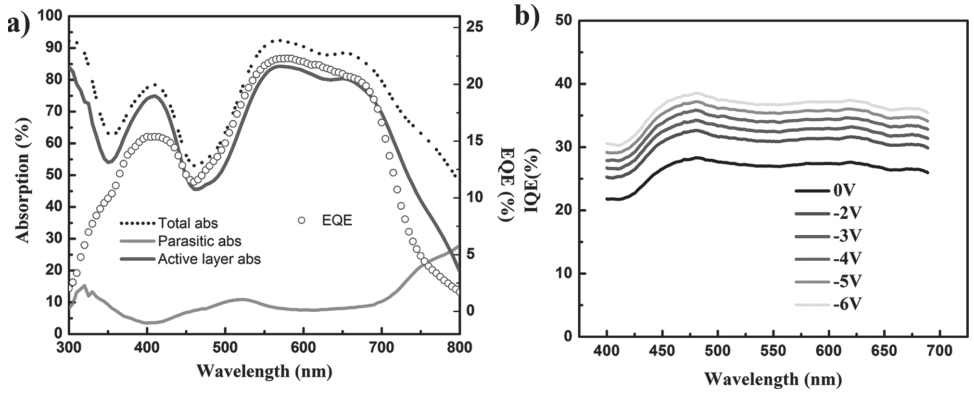

Figure 4. a) Parasitic absorption, active layer absorption and total absorption of *p*-DTS(FBTTh$_2$)$_2$:P(NDI2OD-T2) device as calculated by the transfer matrix optical model along with the EQE of the optimal solar cell device. b) Bias dependent IQE spectrum of optimized *p*-DTS(FBTTh$_2$)$_2$:P(NDI2OD-T2) devices.

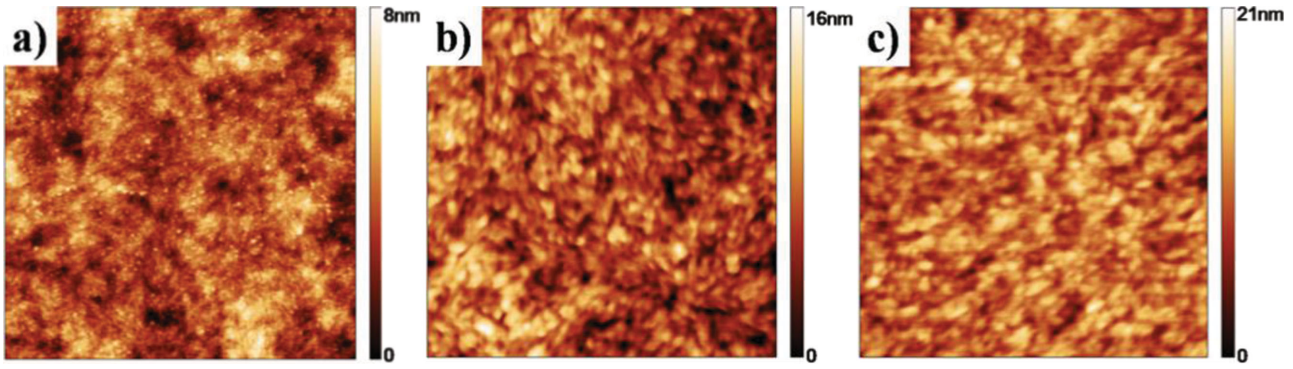

Figure 5. 2 μm × 2 μm AFM topographic images of a) as cast, b) annealed, and c) 0.4% DIO *p*-DTS(FBTTh$_2$)$_2$:P(NDI2OD-T2) cast atop PEDOT:PSS.

(Figure 4b). From IQE measurements under no applied bias, it is found that the IQE of the *p*-DTS(FBTTh$_2$)$_2$:P(NDI2OD-T2) device is only 25%, similar to the EQE value. This similarity implies that absorption does not limit device performance. This relatively low IQE additionally agrees with the ratio of the measured J_{sc} (5.06 mA cm^{-2}) to the maximum theoretical photocurrent (19.6 mA cm^{-2}) calculated using the active layer absorption of *p*-DTS(FBTTh$_2$)$_2$:P(NDI2OD-T2) devices and assuming 100% IQE.[47]

As an initial probe into the origin of the low IQE in *p*-DTS(FBTTh$_2$)$_2$:P(NDI2OD-T2) devices, the IQE was measured as a function of applied bias to understand whether charge generation and extraction may be an issue. As shown in Figure 4b, the IQE of the device increases from 25% to 35% when the bias is further decreased from –2 to –6 V. Additionally, the IQE does not reach a saturation point within the measured bias range. The modest increase in IQE under strong reverse bias may be due to a field dependent charge generation mechanism,[48,49] or the release of trapped charge carriers[21] as the negative bias increases the internal electric field within the device. More notable however, is that even at –6 V the IQE is still <40% suggesting that in addition to a voltage dependent loss mechanism, there are significant losses that are likely independent of voltage. These losses may be from geminate recombination and/or excitons that fail to diffuse to a donor–acceptor interface. Thus, we designed a series of experiments to further investigate the loss mechanisms in *p*-DTS(FBTTh$_2$)$_2$:P(NDI2OD-T2) BHJ OPV devices.

2.2. Morphological Characterization

Atomic force microscopy (AFM) was used to probe the surface morphology of as cast, annealed, and additive processed *p*-DTS(FBTTh$_2$)$_2$:P(NDI2OD-T2) films. As shown in **Figure 5**, the as cast film has a relatively smooth and featureless surface (RMS 3.1 nm); however, upon thermal annealing, one observes fiber-like structures and a higher RMS value, which may imply enhanced crystallinity of the film. Similarly, the additive processed blend film shows some coarser features on the surface with an RMS of ≈6.1 nm. From the AFM images, it is clear that there are no large-scale topographic features present; however, it is difficult to gain insight into the degree of phase separation from tapping-mode AFM measurements alone.

Conducting AFM (c-AFM) is utilized to further investigate the phase separation and conductive domain size of the optimal solar cell devices (**Figure 6**). C-AFM measures surface topography and current simultaneously.[50–59] In c-AFM measurements, a Au-coated Si tip scans over the blend films with an applied voltage between the ITO substrate and the tip. Applying a negative bias to the ITO substrate induces hole injection from tip and hole collection by PEDOT:PSS. The device configuration ITO/PEDOT:PSS/active layer/Au tip resembles the hole-only diode configuration since the work-function of PEDOT:PSS and Au are much closer to the HOMO of *p*-DTS(FBTTh$_2$)$_2$ than the LUMO of either PCBM or P(NDI2OD-T2). As a result, holes are favorably injected to and collected from the *p*-DTS(FBTTh$_2$)$_2$-rich domains, which correlate to the higher current domains in c-AFM images. The size of high current and low current domains, which correspond to donor-rich and acceptor-rich domains, respectively, is determined by the cross-section profile of current images (Supporting Information Figure S8).

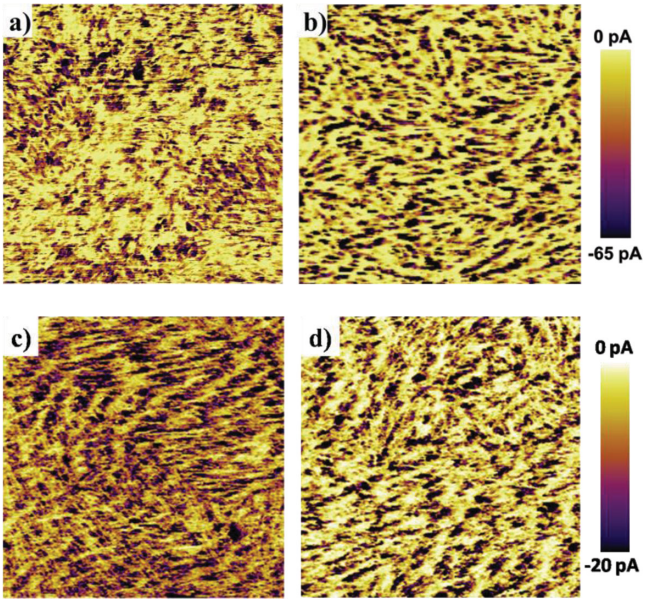

Figure 6. 2 μm × 2 μm scale current images of a) *p*-DTS(FBTTh$_2$)$_2$:PC$_{71}$BM with 0.4% DIO collected at –1 V; b) *p*-DTS(FBTTh$_2$)$_2$:P(NDI2OD-T2) with 0.4% DIO; c) as cast *p*-DTS(FBTTh$_2$)$_2$:P(NDI2OD-T2); d) annealed *p*-DTS(FBTTh$_2$)$_2$:P(NDI2OD-T2) collected at –5 V.

In agreement with the tapping mode images in Figure 5, there is no large micrometer-scale phase separation in as cast, annealed or additive processed *p*-DTS(FBTTh$_2$)$_2$:P(NDI2OD-T2) films. The donor conductive domains are slightly larger than those in *p*-DTS(FBTTh$_2$)$_2$:PC$_{71}$BM. Current image of *p*-DTS(FBTTh$_2$)$_2$:PC$_{71}$BM reveals fiber-like domains with an average size of 13 ± 2 nm, which is consistent with the TEM study by Love et al.[43] Current images of *p*-DTS(FBTTh$_2$)$_2$:P(NDI2OD-T2) as cast and annealed films show much lower conductivity than *p*-DTS(FBTTh$_2$)$_2$:PC$_{71}$BM blend film and relatively larger conductive domain size as 19 ± 7 nm, 21 ± 2 nm, respectively. When using 0.4% DIO, the *p*-DTS(FBTTh$_2$)$_2$:P(NDI2OD-T2) blend film shows higher conductivity and relatively more homogeneous fiber-like domains, with an average size of only 15 ± 1 nm which suggest that the improvement in J_{sc} may be due to the smaller donor domains. Furthermore, the similar domain size of the 0.4% DIO *p*-DTS(FBTTh$_2$)$_2$:PC$_{71}$BM and *p*-DTS(FBTTh$_2$)$_2$:P(NDI2OD-T2) films suggests that the *p*-DTS(FBTTh$_2$)$_2$:P(NDI2OD-T2) system is not limited by large-scale phase separation.

From c-AFM, the conductivity of 0.4% DIO blend is higher than that of as cast and annealed blend films which is consistent with the higher J_{sc} in the device processed with additive. In order to further explain the conductivity and J_{sc} difference between different processing conditions, grazing incidence wide-angle X-ray scattering (GIWAXS) was used to investigate the solid state order and crystalline texture of blend films.[60] As shown in **Figure 7**a, in the as cast blend the (001) and polymorph peak ($q \approx 0.4$, out of plane) of *p*-DTS(FBTTh$_2$)$_2$ are present.[43] P(NDI2OD-T2)'s π–π stacking peak (010), is visible out of plane, indicating a face on orientation to the substrate.[61] Upon adding 0.4% DIO the *p*-DTS(FBTTh$_2$)$_2$ polymorph peak disappears and the higher order *p*-DTS(FBTTh$_2$)$_2$ peaks appear out of plane indicating increased *p*-DTS(FBTTh$_2$)$_2$ solid state order. P(NDI2OD-T2)'s π–π peak also narrows in width upon use of DIO, indicating larger and/or more ordered crystallites compared to the as cast sample. Qualitatively, the annealed blend appears very similar to the blend processed with DIO. GIWAXS then indicates that annealing or processing the blends with DIO increases the solid state order of both donor and acceptor, perhaps in part explaining the increased conductivity and J_{sc} of these blends.

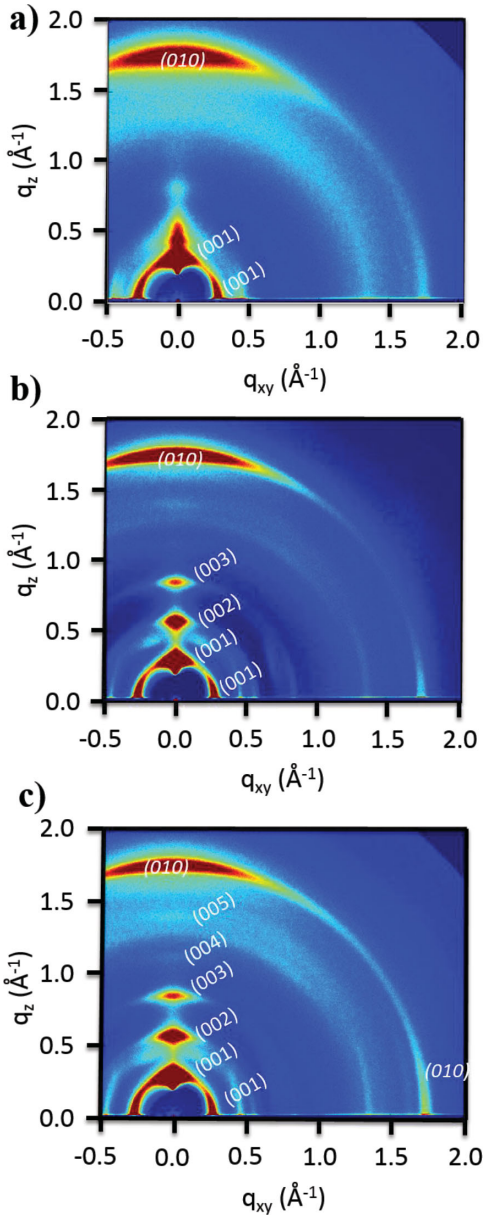

Figure 7. 2D GIWAXS images of *p*-DTS(FBTTh$_2$)$_2$:P(NDI2OD-T2) BHJ films cast atop silicon a) as cast, b) annealed, and c) processed with 0.4% DIO. *p*-DTS(FBTTh$_2$)$_2$ peaks are indexed in italics while the P(NDI2OD-T2) (010) plane is denoted out of plane.

2.3. Charge Transport and Extraction

The charge carrier mobility is another important factor that affects solar cell device performance. Both the electron and hole mobilities are important because if they are too low or imbalanced, charge carriers may recombine before they are collected at the electrodes. This is among the reasons PCBM works well as an acceptor material since its electron mobility is roughly 10^{-3} cm^2 V^{-1} s^{-1}.[62] Pristine P(NDI2OD-T2) has previously been reported to exhibit trap free electron and hole transport with mobilities of 5×10^{-4} cm^2 V^{-1} s^{-1} and 3.4×10^{-6} cm^2 V^{-1} s^{-1}, respectively.[33] To gauge the charge transport properties of *p*-DTS(FBTTh$_2$)$_2$:P(NDI2OD-T2) blends, hole-only and electron-only diodes were fabricated and measured using device geometries of ITO/PEDOT:PSS/blend/Au and Al/blend/LiF/Al, respectively. The hole and electron mobilities of with *p*-DTS(FBTTh$_2$)$_2$:P(NDI2OD-T2) blend processed with 0.4% DIO are 7.5×10^{-5} cm^2 V^{-1} s^{-1} and 7.8×10^{-5} cm^2 V^{-1} s^{-1}, respectively. The *J*–*V* curves of as cast, annealed and additive processed hole- and electron-only devices are shown in Figure S9 of the Supporting Information. When adding DIO or thermal annealing, the electron mobility is increased from 4.3×10^{-5} cm^2 V^{-1} s^{-1} to 7.8×10^{-5} cm^2 V^{-1} s^{-1} and 1.3×10^{-4} cm^2 V^{-1} s^{-1}, respectively, consistent with the increase in P(NDI2OD-T2) solid state order observed with GIWAXS when using additive or thermal annealing. While the electron and hole mobilities in the optimal *p*-DTS(FBTTh$_2$)$_2$:P(NDI2OD-T2)

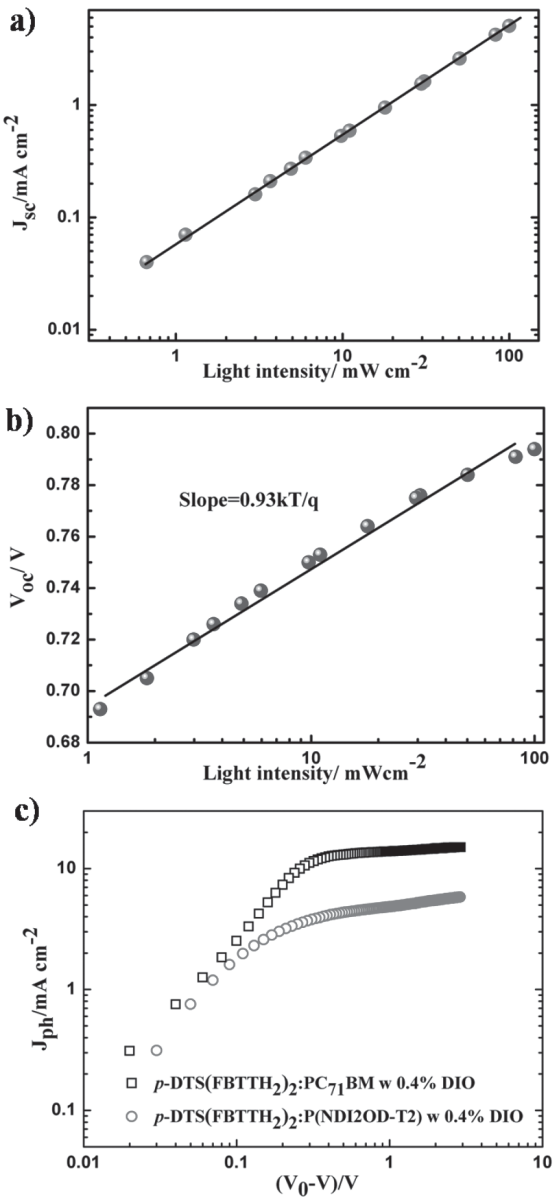

Figure 8. a) Light intensity dependence of J_{sc}. b) Light intensity dependence of V_{oc}. c) Photocurrent versus effective voltage in optimal devices of *p*-DTS(FBTTh$_2$)$_2$:PC$_{71}$BM and *p*-DTS(FBTTh$_2$)$_2$:P(NDI2OD-T2).

blend are well balanced, they are an order of magnitude lower than other high performing organic BHJ solar cell systems. For comparison, the electron mobility and hole mobility of *p*-DTS(FBTTh$_2$)$_2$:PC$_{71}$BM processed with 0.4% DIO are 5×10^{-4} cm^2 V^{-1} s^{-1} and 2×10^{-4} cm^2 V^{-1} s^{-1}.[63] Thus, it is likely that the lower *FF* for *p*-DTS(FBTTh$_2$)$_2$:P(NDI2OD-T2) as compared to *p*-DTS(FBTTh$_2$)$_2$:PC$_{71}$BM (0.53 vs 0.70) is in part due to the lower charge carrier mobilities[64,65,66] which may limit the ability to efficiently extract charges before they recombine.

The dependence of J_{sc} on light intensity was measured to examine if charge transport and nongeminate recombination (bimolecular and trap-assisted recombination) may also significantly limit the J_{sc}. In J_{sc}–light intensity measurements, the J_{sc} should follow a power law relationship as $J_{sc} \sim I^{\alpha}$ where $\alpha < 1.0$ is indicative of significant bimolecular recombination and/or a build up of space-charge.[67] As shown in **Figure 8**a, for the optimized device, J_{sc} scales linearly with light intensity ($\alpha = 1$), which indicates that bimolecular recombination is not a significant loss mechanism at short-circuit. A linear dependence of J_{sc} on light intensity does not preclude the possibility that trap-assisted recombination may be limiting; however, both hole and electron only single carrier diodes exhibited trap-free transport (Supporting Information Figure S9). Furthermore as shown in Figure 8b, the V_{oc} exhibits a logarithmic dependence on light intensity with slope ≈0.93 kT q^{-1}, which indicates that trapping is not a significant loss mechanism.[68,69]

To further understand the charge extraction process, as shown in Figure 8c, a typical *J*–*V* curve is converted to J_{ph}–V_{eff} by plotting the photocurrent with respect to effective voltage which is the voltage at no photocurrent less the applied voltage, V_0–V. The influence of charge extraction dominates at low voltages while the influence of charge generation dominates at high voltages. From J_{ph}–V_{eff} for both devices, at a low effective voltage of around 0.2 V, J_{ph} reaches a plateau suggesting that free charges are swept out efficiently. Thus, it is likely that charge extraction is not a limiting factor for J_{sc}.

At sufficiently high electric fields, J_{ph} of *p*-DTS(FBTTh$_2$)$_2$:PC$_{71}$BM and *p*-DTS(FBTTh$_2$)$_2$:P(NDI2OD-T2) devices show drastic differences. Above 0.2 V, *p*-DTS(FBTTh$_2$)$_2$:PC$_{71}$BM shows a flat plateau and at V_{eff} = 3 V the photocurrent is ≈15 mA cm^{-2}. For *p*-DTS(FBTTh$_2$)$_2$:P(NDI2OD-T2), the photocurrent does not saturate and increases modestly with higher bias. In addition, at V_{eff} = 3 V, the photocurrent of *p*-DTS(FBTTh$_2$)$_2$:P(NDI2OD-T2) is only ≈5.5 mA cm^{-2}. The difference in the saturation region shows that compared to *p*-DTS(FBTTh$_2$)$_2$:PC$_{71}$BM, fewer charges are generated. All together, these findings support the conclusions drawn from the IQE measurements that the primary loss mechanism limiting the J_{sc} is mostly likely related to charge generation.

2.4. Exciton Diffusion

Charge generation in donor:acceptor solar cells occurs via a multistep process: after photoexcitation of the donor (or acceptor), excitons diffuse toward the donor:acceptor interface, where they can separate into free charges directly, via ultrafast dissociation, or through an intermediate state, usually referred to as charge transfer (CT) state.[70,71] The latter consists of a Coulombically bound electron and hole pair at the donor:acceptor interface, with a binding energy of about 0.1 to 0.5 eV.[71,72] The overall process of charge generation requires dissociation of these initially photogenerated bound electron-hole pairs into free charge carriers, which can then be transported to and collected by the device electrodes. The term "free carrier" used here refers to the yield of fully dissociated (i.e., free) charges. Considering that the Coulomb binding energy is significantly larger than room temperature thermal energy, k_BT, an energy offset between LUMO energy levels of donor and acceptor material is necessary for electron transfer to take place. Both PC$_{71}$BM and P(NDI2OD-T2) have similar LUMO energies, making electron transfer energetically favorable in both systems (Figure 1).

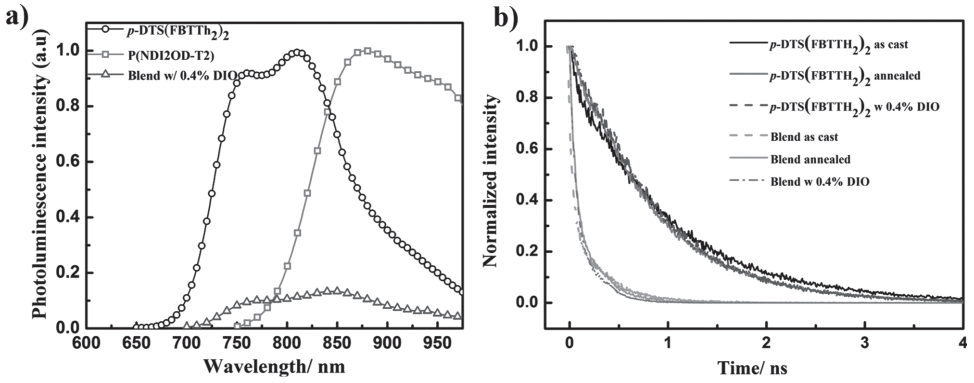

Figure 9. a) Photoluminescence of pristine *p*-DTS(FBTTh$_2$)$_2$ and P(NDI2OD-T2) films and blend normalized by absorption intensity. b) Time-resolved photoluminescence of *p*-DTS(FBTTh$_2$)$_2$ and as cast, annealed, and additive processed *p*-DTS(FBTTh$_2$)$_2$ blend films.

As mentioned previously P(NDI2OD-T2) has much stronger absorption in the visible when compared to $PC_{71}BM$, yielding the possibility of enhanced J_{sc} in devices. However, the smaller band gap consequently leads to a smaller HOMO-HOMO offset 0.32 eV for *p*-DTS(FBTTh$_2$)$_2$:P(NDI2OD-T2) compared to >0.6 eV for *p*-DTS(FBTTh$_2$)$_2$:$PC_{71}BM$. While 0.3 eV is often cited in the literature as the threshold energy level offset needed for efficient charge generation, it is worth noting that this remains an area of active research and thus it is not clear what effect, if any, the smaller offset present here may have on the charge generation process. Nonetheless, for the hole transfer process to occur at the *p*-DTS(FBTTh$_2$)$_2$:P(NDI2OD-T2) interface, it first requires that excitons from P(NDI2OD-T2) diffuse to that interface. Thus, we attempted to measure the exciton diffusion length using photoluminescence (PL) quenching measurements.[73]

To probe the behavior of excited states in our system, we explore the steady-state PL quenching efficiency in blends and the exciton diffusion length of pristine P(NDI2OD-T2). Geminate recombination of the initially generated CT states back to the ground state may compete with dissociation of these charges into free charge carriers.[74] One simple method to investigate whether excitons in both materials successfully reach the interface is a PL quenching measurement. By studying the time-resolved PL of the *p*-DTS(FBTTh$_2$)$_2$:P(NDI2OD-T2) blend film along with the pristine films, the quenching efficiency of each material in the blend can be calculated using Equation S1 in the Supporting Information. The static PL spectra of *p*-DTS(FBTTh$_2$)$_2$ and P(NDI2OD-T2) overlap above 775 nm (**Figure 9**a). However, at 750 nm, the PL emission is only from *p*-DTS(FBTTh$_2$)$_2$. Thus, to rule out the effect of the PL from P(NDI2OD-T2), the emission at 750 nm was measured in *p*-DTS(FBTTh$_2$)$_2$ pristine film and blend film. In Figure 9a, the PL of the blend is significantly quenched compared to pristine *p*-DTS(FBTTh$_2$)$_2$ and from 750 nm, quenching efficiency is calculated as 83.1%. In Figure 9b, the time-resolved PL of blend films under different conditions are all quenched by P(NDI2OD-T2) which is consistent with the static PL spectra in Figure 9a. This observation indicates efficient charge transfer from donor to acceptor. The quenching efficiencies of as cast, annealed, and additive processed BHJ blend films are 83.2%, 83.0% and 84.4% respectively. Optimized additive processed *p*-DTS(FBTTh$_2$)$_2$:$PC_{71}BM$ BHJ OPV blends have a quenching efficiency of 83.4%, similar to the *p*-DTS(FBTTh$_2$)$_2$:P(NDI2OD-T2) blend films. The relatively high quenching efficiency in optimized device is consistent the fine phase separation observed by AFM. Conclusively, it is evident that in *p*-DTS(FBTTh$_2$)$_2$:P(NDI2OD-T2) blend films most excitons generated in *p*-DTS(FBTTh$_2$)$_2$ are able to diffuse to the D:A interface.

From the static PL spectra of *p*-DTS(FBTTh$_2$)$_2$ and P(NDI2OD-T2) in Figure 9a, it is obvious that it is difficult to decouple P(NDI2OD-T2)'s PL spectrum from that of *p*-DTS(FBTTh$_2$)$_2$ making it infeasible to study the exciton diffusion in P(NDI2OD-T2) by the PL quenching method. Another method used to measure exciton diffusion length is to model the EQE of a bilayer device.[75–79] However, this methodology is impractical in the current case as both *p*-DTS(FBTTh$_2$)$_2$ and P(NDI2OD-T2) are soluble in common organic solvents, preventing the fabrication of a bilayer with an abrupt donor–acceptor interface. Thus, we estimate the P(NDI2OD-T2) exciton diffusion length using Förster resonant energy transfer (FRET) theory. For conjugated materials, it is well established that exciton diffusion occurs through a hopping mechanism. Because of the exponential attenuation of overlap of the donor and acceptor molecular orbitals with distance between molecules, contributions from Dexter energy transfer are normally negligible. The efficiency of this type of energy transfer process can be calculated from FRET theory.[80–83] In FRET theory the exciton diffusion coefficient can be calculated from the spectral overlap of the absorption and emission of the chromophores. With an inter-chromophore distance R, the diffusion process is simplified as a 3D random walk with six nearest neighbor chromophores and the diffusion coefficient is expressed as:[84]

$$D = \frac{R^2}{6\tau_{hop}} \quad (1)$$

In Equation (1), τ_{hop} is exciton hopping lifetime and can be calculated from FRET theory

$$\tau_{hop} = \tau\left(\frac{R}{R_0}\right)^6 \quad (2)$$

where τ is the fluorescence lifetime in film and R_0 is the Förster radius which was calculated from the extinction coefficient and area normalized PL spectra shown in Supporting Information Figure S10b. R is estimated by assuming chromophores are positioned in cubic lattice using Supporting Information Equation S2. The Förster radius R_0 is calculated from the spectral overlap of absorption and emission using:[85]

$$R_0^6 = \frac{9000(\ln 10)k^2 QY}{128\pi^5 N_A n^4}\int_0^\infty F(\lambda)\varepsilon(\lambda)\lambda^4 \mathrm{d}\lambda, \quad (3)$$

where k^2 is the relative orientation of dipoles (k^2 = 0.476 assuming rigid and randomly oriented dipoles),[86] QY is the PL quantum yield in film, n is the average refractive index of the medium in the wavelength range at which spectral overlap is significant, $\varepsilon(\lambda)$ is the molar extinction coefficient in film which was obtained using spectral ellipsometry as shown in Supporting Information Figure S10a, and $F(\lambda)$ is the corrected fluorescence intensity of the film with the area normalized to unity. The exciton diffusion length (L) easily follows from the above calculations, as shown in Equation (4).

$$L = \sqrt{D\tau} \quad (4)$$

For P(NDI2OD-T2) films, the PL quantum yield is too low to detect by our home-built fluorimeter (see Supporting Information). Therefore, we cannot calculate the exact value of the exciton diffusion coefficient nor the exciton diffusion length in P(NDI2OD-T2) films. The low PL quantum yield and PL lifetime could be the result of intrinsic material properties or exciton traps.[87,88] However, in dilute solution, chain aggregation and interchain hopping are significantly reduced and excitons have fewer chances to encounter defects or traps. Thus, the solution PL quantum yield is measured as an estimate of the potential maximum values of QY and the exciton diffusion length of P(NDI2OD-T2). For the measurement of the QY value of P(NDI2OD-T2) in solution, chloronaphthalene (CN) is used as the solvent since P(NDI2OD-T2) tends to preaggregate in most solvents, including chlorobenzene, while it does not aggregate in dilute concentrations in CN.[89] Therefore, to minimize any aggregation in solution, a low concentration of P(NDI2OD-T2) (4×10^{-3} mg mL^{-1}) in CN was used for measurement of QY. Even in dilute solution, the PL quantum yield of P(NDI2OD-T2) is only 0.8%, which should be considered as the upper limit for the film QY.

The solution PL lifetime in CN is 198 ps, similar to that of the film (Supporting Information Figure S11). The very low PL QY and short PL lifetime may be intrinsic properties of P(NDI2OD-T2). According to Equation (3), the upper limit of the Förster radius R_0 is calculated as 1.37 nm by using the solution PL quantum yield and lifetime values. From Equations (1), (2) and (4), the upper limit of the exciton diffusion length is then determined to be 1.1 nm, significantly shorter than most other studied organic semiconductors (5–10 nm).[73,87,90,91] With such a short exciton diffusion length, excitons generated in the P(NDI2OD-T2) phase may not be able to reach the donor:acceptor interface resulting in photocurrent losses. This is especially noteworthy as the absorption spectra of p-DTS(FBTTh$_2$)$_2$ and P(NDI2OD-T2) overlap, thus leading to competition between donor and acceptor for absorption of incident photons. The short exciton diffusion length of excitons originating on P(NDI2OD-T2) is therefore likely a significant cause of the relatively low J_{sc} observed in p-DTS(FBTTh$_2$)$_2$:P(NDI2OD-T2) BHJ OPV devices. The extremely short P(NDI2OD-T2) exciton diffusion length calculated here is also consistent with the negligible EQE in the wavelength region associated with P(NDI2OD-T2) absorption in previously reported polymer:polymer BHJ OPV blends.[37,92]

3. Conclusion

Due to the desirable electronic and optical properties of P(NDI2OD-T2), we have used it as an alternative electron acceptor to PC$_{71}$BM in combination with the molecular donor p-DTS(FBTTh$_2$)$_2$. By using a small molecule donor, we hoped to avoid the development of large-scale phase separation that has been identified as a limiting factor in blends of polymeric donors with P(NDI2OD-T2). Despite the promising morphological properties of blend films, the optimized devices yield a relatively low PCE of 2.11%. The low PCE of p-DTS(FBTTh$_2$)$_2$:P(NDI2OD-T2) BHJ OPV devices is primarily caused by low J_{sc} in combination with a reduced FF relative to the analogous PC$_{71}$BM blends. Single-carrier diodes of the optimized p-DTS(FBTTh$_2$)$_2$:P(NDI2OD-T2) blend films revealed that the reduced FF may be the result of lower hole and electron mobilities. More importantly, the significantly reduced J_{sc} relative to devices with PC$_{71}$BM as an electron acceptor could be explained by the very short exciton diffusion length of P(NDI2OD-T2) (≈1.1 nm) as compared to PC$_{71}$BM (>5 nm).[76] This results in inefficient exciton harvesting, which is exacerbated due to the competitive absorption between donor and acceptor, leading to a very low J_{sc}.

This comprehensive combination of optical and electronic characterization leads us to conclude that the very short exciton diffusion length of P(NDI2OD-T2) is an intrinsic limitation of the material that puts a ceiling on the performance of BHJ OPVs that use it as an acceptor. This limitation is quite different than that of perylene diimide (PDI) acceptor blended with p-DTS(FBTTh$_2$)$_2$, in which, lower device performance is primarily limited by some combination of charge trapping and geminate recombination.[21,30] It differes from other nonfullerene acceptors as well: diketopyrrolopyrrole based acceptors, have yielded low PCEs to date because of the more compact aromatic surface, which diminishes aggregation of the acceptor and thereby inhibits electron transport in the blend film;[93,94] pentacene acceptors suffer from over crystallization resulting in poor charge separation;[95,96] carbazole acceptors, have yielded low fill factors and current mainly due to the limited electron mobility.[97] Therefore, to realize BHJ OPVs with PCEs equivalent to or surpassing those of devices with PCBM utilizing nonfullerene, new structures must be synthesized that not only have superior exciton diffusion lengths and electron mobility but also reduced geminate recombination and controllable phase separation. Recently Zhou et al. and Earmme et al. both used n-type acceptors structurally similar to P(NDI2OD-T2) and achieved PCE of 4.21% and 4.8% respectively.[20,98] Inspired by these successful examples, the future development of non-fullerene acceptors based on P(NDI2OD-T2) should consider chemical

modifications to increase exciton diffusion lengths while still maintaining trap-free transport and high electron mobility.

Supporting Information

Supporting Information is available from the Wiley Online Library or from the author.

Acknowledgements

The authors are grateful for financial support from the National Science Foundation, SOLAR program (DMR-1035480, exciton diffusion study) and the Office of Naval Research (charge transport and recombination). T.Q.N. thanks the Camille Dreyfus Teacher Scholar Award. C.P. and A.S. acknowledge support from the National Science Foundation Graduate Research Fellowship Program under Grant No. DGE-1144085. The authors also thank Dr. Alexander Mikhailovsky for the help with the photoluminescence measurement. Portions of this research were conducted at the Stanford Synchrotron Radiation Lightsource user facility, operated by Stanford University on behalf of the U.S. Department of Energy, Office of Basic Energy Sciences. Use of the Stanford Synchrotron Radiation Lightsource, SLAC National Accelerator Laboratory, is supported by the U.S. Department of Energy, Office of Science, Office of Basic Energy Sciences under Contract No. DE-AC02–76SF00515.

Received: April 28, 2014
Revised: July 18, 2014
Published online: September 2, 2014

[1] B. Walker, A. B. Tamayo, X.-D. Dang, P. Zalar, J. H. Seo, A. Garcia, M. Tantiwiwat, T.-Q. Nguyen, *Adv. Funct. Mater.* **2009**, *19*, 3063.
[2] T. S. van der Poll, J. A. Love, T.-Q. Nguyen, G. C. Bazan, *Adv. Mater.* **2012**, *24*, 3646.
[3] J. Zhou, Y. Zuo, X. Wan, G. Long, Q. Zhang, W. Ni, Y. Liu, Z. Li, G. He, C. Li, B. Kan, M. Li, Y. Chen, *J. Am. Chem. Soc.* **2013**, *135*, 8484.
[4] A. K. K. Kyaw, D. H. Wang, V. Gupta, J. Zhang, S. Chand, G. C. Bazan, A. J. Heeger, *Adv. Mater.* **2013**, *25*, 2397.
[5] L. G. Mercier, A. Mishra, Y. Ishigaki, F. Henne, G. Schulz, P. Bäuerle, *Org. Lett.* **2014**, *16*, 2642.
[6] S. Loser, H. Miyauchi, J. W. Hennek, J. Smith, C. Huang, A. Facchetti, T. J. Marks, *Chem. Commun.* **2012**, *48*, 8511.
[7] O. P. Lee, A. T. Yiu, P. M. Beaujuge, C. H. Woo, T. W. Holcombe, J. E. Millstone, J. D. Douglas, M. S. Chen, J. M. J. Fréchet, *Adv. Mater.* **2011**, *23*, 5359.
[8] Y. Liu, C.-C. Chen, Z. Hong, J. Gao, Y. (M.) Yang, H. Zhou, L. Dou, G. Li, Y. Yang, *Sci. Rep.* **2013**, *3*, 1.
[9] J. Roncali, P. Leriche, P. Blanchard, *Adv. Mater.* **2014**, *26*, 3821.
[10] Z. Li, G. He, X. Wan, Y. Liu, J. Zhou, G. Long, Y. Zuo, M. Zhang, Y. Chen, *Adv. Energy Mater.* **2012**, *2*, 74.
[11] Y. Lin, L. Ma, Y. Li, Y. Liu, D. Zhu, X. Zhan, *Adv. Energy Mater.* **2013**, *3*, 1166.
[12] Y. J. Kim, J. Y. Baek, J. Ha, D. S. Chung, S.-K. Kwon, C. E. Park, Y.-H. Kim, *J. Mater. Chem. C* **2014**, *2*, 4937.
[13] H. Qin, L. Li, F. Guo, S. Su, J. Peng, Y. Cao, X. Peng, *Energy Environ. Sci.* **2014**, *7*, 1397.
[14] N. C. Cates, R. Gysel, Z. Beiley, C. E. Miller, M. F. Toney, M. Heeney, I. McCulloch, M. D. McGehee, *Nano Lett.* **2009**, *9*, 4153.
[15] J. Kalowekamo, E. Baker, *Sol. Energy* **2009**, *83*, 1224.
[16] T. D. Nielsen, C. Cruickshank, S. Foged, J. Thorsen, F. C. Krebs, *Sol. Energy Mater. Sol. Cells* **2010**, *94*, 1553.
[17] A. Anctil, C. W. Babbitt, R. P. Raffaelle, B. J. Landi, *Environ. Sci. Technol.* **2011**, *45*, 2353.
[18] Y. Yao, C. Shi, G. Li, V. Shrotriya, Q. Pei, Y. Yang, *Appl. Phys. Lett.* **2006**, *89*, 153507.
[19] E. Zhou, J. Cong, K. Hashimoto, K. Tajima, *Adv. Mater.* **2013**, *25*, 6991.
[20] Y. Zhou, T. Kurosawa, W. Ma, Y. Guo, L. Fang, K. Vandewal, Y. Diao, C. Wang, Q. Yan, J. Reinspach, J. Mei, A. L. Appleton, G. I. Koleilat, Y. Gao, S. C. B. Mannsfeld, A. Salleo, H. Ade, D. Zhao, Z. Bao, *Adv. Mater.* **2014**, *26*, 3767.
[21] A. Sharenko, C. M. Proctor, T. S. van der Poll, Z. B. Henson, T.-Q. Nguyen, G. C. Bazan, *Adv. Mater.* **2013**, *25*, 4403.
[22] G. D. Sharma, M. S. Roy, J. A. Mikroyannidis, K. R. Justin Thomas, *Org. Electron.* **2012**, *13*, 3118.
[23] J. T. Bloking, X. Han, A. T. Higgs, J. P. Kastrop, L. Pandey, J. E. Norton, C. Risko, C. E. Chen, J.-L. Brédas, M. D. McGehee, A. Sellinger, *Chem. Mater.* **2011**, *23*, 5484.
[24] T. W. Holcombe, J. E. Norton, J. Rivnay, C. H. Woo, L. Goris, C. Piliego, G. Griffini, A. Sellinger, J.-L. Brédas, A. Salleo, J. M. J. Fréchet, *J. Am. Chem. Soc.* **2011**, *133*, 112106.
[25] E. Zhou, J. Cong, Q. Wei, K. Tajima, C. Yang, K. Hashimoto, *Angew. Chem. Int. Ed.* **2011**, *50*, 2799.
[26] G. D. Sharma, P. Balraju, J. A. Mikroyannidis, M. M. Stylianakis, *Sol. Energy Mater. Sol. Cells* **2009**, *93*, 2025.
[27] J. A. Mikroyannidis, P. Suresh, G. D. Sharma, *Synth. Met.* **2010**, *160*, 932.
[28] N. Camaioni, G. Ridolfi, V. Fattori, L. Favaretto, G. Barbarella, *Appl. Phys. Lett.* **2004**, *84*, 1901.
[29] D. A. M. Egbe, T. Kietzke, B. Carbonnier, D. Mühlbacher, H.-H. Hörhold, D. Neher, T. Pakula, *Macromolecules* **2004**, *37*, 8863.
[30] A. Sharenko, D. Gehrig, F. Laquai, T.-Q. Nguyen, *Chem. Mater.* **2014**, *26*, 4109.
[31] Z. Chen, Y. Zheng, H. Yan, A. Facchetti, *J. Am. Chem. Soc.* **2009**, *131*, 8.
[32] H. Yan, Z. Chen, Y. Zheng, C. Newman, J. R. Quinn, F. Dötz, M. Kastler, A. Facchetti, *Nature* **2009**, *457*, 679.
[33] G.-J. A. H. Wetzelaer, M. Kuik, Y. Olivier, V. Lemaur, J. Cornil, S. Fabiano, M. A. Loi, P. W. M. Blom, *Phys. Rev. B* **2012**, *86*, 165203.
[34] J. M. Leng, X. Wei, Z. V. Vardeny, K. C. Khemani, D. Moses, F. Wudl, *Phys. Rev. B* **1993**, *48*, 18250.
[35] W. Zhang, Z. Tan, D. Qian, L. Li, Q. Xu, S. Li, H. Zheng, Y. Li, *J. Phys. Appl. Phys.* **2012**, *45*, 285102.
[36] Y. Tang, C. R. McNeill, *J. Polym. Sci. Part B Polym. Phys.* **2013**, *51*, 403.
[37] S. Fabiano, Z. Chen, S. Vahedi, A. Facchetti, B. Pignataro, M. A. Loi, *J. Mater. Chem.* **2011**, *21*, 5891.
[38] N. Zhou, H. Lin, S. J. Lou, X. Yu, P. Guo, E. F. Manley, S. Loser, P. Hartnett, H. Huang, M. R. Wasielewski, L. X. Chen, R. P. H. Chang, A. Facchetti, T. J. Marks, *Adv. Energy Mater.* **2014**, *4*, 1300785.
[39] M. Schubert, D. Dolfen, J. Frisch, S. Roland, R. Steyrleuthner, B. Stiller, Z. Chen, U. Scherf, N. Koch, A. Facchetti, D. Neher, *Adv. Energy Mater.* **2012**, *2*, 369.
[40] H. Yan, B. A. Collins, E. Gann, C. Wang, H. Ade, C. R. McNeill, *ACS Nano* **2012**, *6*, 677.
[41] B. H. Wunsch, K. Kim, Y. Rho, B. Ahn, S. Jung, L. E. Polander, D. G. Bucknall, S. R. Marder, M. Ree, *J. Mater. Chem. C* **2012**, *1*, 778.
[42] A. K. K. Kyaw, D. H. Wang, V. Gupta, W. L. Leong, L. Ke, G. C. Bazan, A. J. Heeger, *ACS Nano* **2013**, *7*, 4569.
[43] J. A. Love, C. M. Proctor, J. Liu, C. J. Takacs, A. Sharenko, T. S. van der Poll, A. J. Heeger, G. C. Bazan, T.-Q. Nguyen, *Adv. Funct. Mater.* **2013**, *23*, 5019.

[44] D. H. Wang, A. K. K. Kyaw, V. Gupta, G. C. Bazan, A. J. Heeger, *Adv. Energy Mater.* **2013**, *3*, 1161.
[45] T. Rath, V. Kaltenhauser, W. Haas, A. Reichmann, F. Hofer, G. Trimmel, *Sol. Energy Mater. Sol. Cells* **2013**, *114*, 38.
[46] P. Zalar, M. Kuik, N. A. Ran, J. A. Love, T.-Q. Nguyen, *Adv. Energy Mater.* **2014**, DOI: 10.1002/aenm.201400438.
[47] G. F. Burkhard, E. T. Hoke, M. D. McGehee, *Adv. Mater.* **2010**, *22*, 3293.
[48] S. Albrecht, W. Schindler, J. Kurpiers, J. Kniepert, J. C. Blakesley, I. Dumsch, S. Allard, K. Fostiropoulos, U. Scherf, D. Neher, *J. Phys. Chem. Lett.* **2012**, *3*, 640.
[49] J. Kniepert, M. Schubert, J. C. Blakesley, D. Neher, *J. Phys. Chem. Lett.* **2011**, *2*, 700.
[50] O. G. Reid, K. Munechika, D. S. Ginger, *Nano Lett.* **2008**, *8*, 1602.
[51] M. Guide, X.-D. Dang, T.-Q. Nguyen, *Adv. Mater.* **2011**, *23*, 2313.
[52] O. Douhéret, L. Lutsen, A. Swinnen, M. Breselge, K. Vandewal, L. Goris, J. Manca, *Appl. Phys. Lett.* **2006**, *89*, 032107.
[53] Z. He, H. Phan, J. Liu, T.-Q. Nguyen, T. T. Y. Tan, *Adv. Mater.* **2013**, *25*, 6900.
[54] W. C. Tsoi, P. G. Nicholson, J. S. Kim, D. Roy, T. L. Burnett, C. E. Murphy, J. Nelson, D. D. C. Bradley, J.-S. Kim, F. A. Castro, *Energy Environ. Sci.* **2011**, *4*, 3646.
[55] M. Dante, C. Yang, B. Walker, F. Wudl, T.-Q. Nguyen, *Adv. Mater.* **2010**, *22*, 1835.
[56] X.-D. Dang, A. B. Tamayo, J. Seo, C. V. Hoven, B. Walker, T.-Q. Nguyen, *Adv. Funct. Mater.* **2010**, *20*, 3314.
[57] X.-D. Dang, M. Dante, T.-Q. Nguyen, *Appl. Phys. Lett.* **2008**, *93*, 241911.
[58] D. C. Coffey, O. G. Reid, D. B. Rodovsky, G. P. Bartholomew, D. S. Ginger, *Nano Lett.* **2007**, *7*, 738.
[59] D. J. Wold, C. D. Frisbie, *J. Am. Chem. Soc.* **2001**, *123*, 5549.
[60] P. Müller-Buschbaum, *Adv. Mater.* **2014**, DOI: 10.1002/adma.201304187.
[61] J. Rivnay, R. Steyrleuthner, L. H. Jimison, A. Casadei, Z. Chen, M. F. Toney, A. Facchetti, D. Neher, A. Salleo, *Macromolecules* **2011**, *44*, 5246.
[62] J. Nakamura, K. Murata, K. Takahashi, *Appl. Phys. Lett.* **2005**, *87*, 132105.
[63] C. M. Proctor, S. Albrecht, M. Kuik, D. Neher, T.-Q. Nguyen, *Adv. Energy Mater.* **2014**, *4*, 1400230.
[64] C. M. Proctor, J. A. Love, T.-Q. Nguyen, *Adv. Mater.* **2014**, DOI: 10.1002/adma.201401725.
[65] C. M. Proctor, C. Kim, D. Neher, T.-Q. Nguyen, *Adv. Funct. Mater.* **2013**, *23*, 3584.
[66] A. Baumann, J. Lorrmann, D. Rauh, C. Deibel, V. Dyakonov, *Adv. Mater.* **2012**, *24*, 4381.
[67] L. J. A. Koster, V. D. Mihailetchi, H. Xie, P. W. M. Blom, *Appl. Phys. Lett.* **2005**, *87*, 203502.
[68] L. J. A. Koster, V. D. Mihailetchi, R. Ramaker, P. W. M. Blom, *Appl. Phys. Lett.* **2005**, *86*, 123509.
[69] S. R. Cowan, A. Roy, A. J. Heeger, *Phys. Rev. B* **2010**, *82*, 245207.
[70] C. Deibel, V. Dyakonov, *Rep. Prog. Phys.* **2010**, *73*, 096401.
[71] A. A. Bakulin, A. Rao, V. G. Pavelyev, P. H. M. van Loosdrecht, M. S. Pshenichnikov, D. Niedzialek, J. Cornil, D. Beljonne, R. H. Friend, *Science* **2012**, *335*, 1340.
[72] T. M. Clarke, J. R. Durrant, *Chem. Rev.* **2010**, *110*, 6736.
[73] J. D. A. Lin, O. V. Mikhnenko, J. Chen, Z. Masri, A. Ruseckas, A. Mikhailovsky, R. P. Raab, J. Liu, P. W. M. Blom, M. A. Loi, C. J. García-Cervera, I. D. W. Samuel, T.-Q. Nguyen, *Mater. Horiz.* **2014**, *1*, 280.
[74] C. M. Proctor, M. Kuik, T.-Q. Nguyen, *Prog. Polym. Sci.* **2013**, *38*, 1941.
[75] J. Wagner, T. Fritz, H. Böttcher, *Phys. Status Solidi A* **1993**, *136*, 423.
[76] L. A. A. Pettersson, L. S. Roman, O. Inganäs, *J. Appl. Phys.* **1999**, *86*, 487.
[77] M. Theander, A. Yartsev, D. Zigmantas, V. Sundström, W. Mammo, M. R. Andersson, O. Inganäs, *Phys. Rev. B* **2000**, *61*, 12957.
[78] P. Peumans, A. Yakimov, S. R. Forrest, *J. Appl. Phys.* **2003**, *93*, 3693.
[79] D. Qin, P. Gu, R. S. Dhar, S. G. Razavipour, D. Ban, *Phys. Status Solidi A* **2011**, *208*, 1967.
[80] I. Hwang, G. D. Scholes, *Chem. Mater.* **2011**, *23*, 610.
[81] R. Signerski, G. Jarosz, *Photonics Lett. Pol.* **2011**, *3*, 107.
[82] R. R. Lunt, J. B. Benziger, S. R. Forrest, *Adv. Mater.* **2010**, *22*, 1233.
[83] T. K. Mullenbach, K. A. McGarry, W. A. Luhman, C. J. Douglas, R. J. Holmes, *Adv. Mater.* **2013**, *25*, 3689.
[84] R. C. Powell, Z. G. Soos, *J. Lumin.* **1975**, *11*, 1.
[85] T. Förster, *Ann. Phys.* **1948**, *437*, 55.
[86] I. Z. Steinberg, *Annu. Rev. Biochem.* **1971**, *40*, 83.
[87] O. V. Mikhnenko, M. Kuik, J. Lin, N. van der Kaap, T.-Q. Nguyen, P. W. M. Blom, *Adv. Mater.* **2014**, *26*, 1912.
[88] R. F. Fink, J. Seibt, V. Engel, M. Renz, M. Kaupp, S. Lochbrunner, H.-M. Zhao, J. Pfister, F. Würthner, B. Engels, *J. Am. Chem. Soc.* **2008**, *130*, 12858.
[89] R. Steyrleuthner, M. Schubert, I. Howard, B. Klaumünzer, K. Schilling, Z. Chen, P. Saalfrank, F. Laquai, A. Facchetti, D. Neher, *J. Am. Chem. Soc.* **2012**, *134*, 18303.
[90] S. Cook, A. Furube, R. Katoh, L. Han, *Chem. Phys. Lett.* **2009**, *478*, 33.
[91] J. D. A. Lin, J. Liu, C. Kim, A. B. Tamayo, C. M. Proctor, T.-Q. T. Nguyen, *RSC Adv.* **2014**, *4*, 14101.
[92] J. R. Moore, S. Albert-Seifried, A. Rao, S. Massip, B. Watts, D. J. Morgan, R. H. Friend, C. R. McNeill, H. Sirringhaus, *Adv. Energy Mater.* **2011**, *1*, 230.
[93] P. Sonar, G.-M. Ng, T. T. Lin, A. Dodabalapur, Z.-K. Chen, *J. Mater. Chem.* **2010**, *20*, 3626.
[94] B. P. Karsten, J. C. Bijleveld, R. A. J. Janssen, *Macromol. Rapid Commun.* **2010**, *31*, 1554.
[95] Y.-F. Lim, Y. Shu, S. R. Parkin, J. E. Anthony, G. G. Malliaras, *J. Mater. Chem.* **2009**, *19*, 3049.
[96] Y. Shu, Y.-F. Lim, Z. Li, B. Purushothaman, R. Hallani, J. E. Kim, S. R. Parkin, G. G. Malliaras, J. E. Anthony, *Chem. Sci.* **2011**, *2*, 363.
[97] Y. Zhou, J. Pei, Q. Dong, X. Sun, Y. Liu, W. Tian, *J. Phys. Chem. C* **2009**, *113*, 7882.
[98] T. Earmme, Y.-J. Hwang, S. Subramaniyan, S. A. Jenekhe, *Adv. Mater.* **2014**, DOI: 10.1002/adma.201401490.